# Effect of particle shape and slip mechanism on buoyancy induced convective heat transport with nanofluids

Pranit Satish Joshi, Pallab Sinha Mahapatra, and Arvind Pattamatta

Citation: Physics of Fluids **29**, 122001 (2017);
View online: https://doi.org/10.1063/1.4996824
View Table of Contents: http://aip.scitation.org/toc/phf/29/12
Published by the American Institute of Physics

# Effect of particle shape and slip mechanism on buoyancy induced convective heat transport with nanofluids

Pranit Satish Joshi, Pallab Sinha Mahapatra,[a] and Arvind Pattamatta
*Department of Mechanical Engineering, Indian Institute of Technology Madras, Chennai 600036, India*

(Received 19 July 2017; accepted 14 November 2017; published online 7 December 2017)

Experiments and numerical simulation of natural convection heat transfer with nanosuspensions are presented in this work. The investigations are carried out for three different types of nanosuspensions: namely, spherical-based (alumina/water), tubular-based (multi-walled carbon nanotube/water), and flake-based (graphene/water). A comparison with in-house experiments is made for all the three nanosuspensions at different volume fractions and for the Rayleigh numbers in the range of $7 \times 10^5$–$1 \times 10^7$. Different models such as single component homogeneous, single component non-homogeneous, and multicomponent non-homogeneous are used in the present study. From the present numerical investigation, it is observed that for lower volume fractions (~0.1%) of nanosuspensions considered, single component models are in close agreement with the experimental results. Single component models which are based on the effective properties of the nanosuspensions alone can predict heat transfer characteristics very well within the experimental uncertainty. Whereas for higher volume fractions (~0.5%), the multi-component model predicts closer results to the experimental observation as it incorporates drag-based slip force which becomes prominent. The enhancement observed at lower volume fractions for non-spherical particles is attributed to the percolation chain formation, which perturbs the boundary layer and thereby increases the local Nusselt number values. *Published by AIP Publishing.* https://doi.org/10.1063/1.4996824

## I. INTRODUCTION

In recent times, convective heat transfer in nanosuspensions has become a very active field of research. Anomalously high thermal conductivity, less pressure drop, and stability in suspension are some of the interesting properties of nanosuspensions (nanofluids) over conventional slurries.[1–5] The surge in the power density of electronic equipment due to miniaturization cannot suffice the need by conventional coolants alone. In addition to increase in thermal conductivity, researchers had also observed high heat transfer coefficient in the forced convection studies. However, experimental studies on natural convection using nanofluids are relatively scarce.[6–13] It is seen from the available literature[6,7,9,11–13] that addition of the nanoparticles in a basefluid deteriorates the heat transfer. Also, there have been great discrepancies in the numerical results when compared with the experiments in natural convection studies with nanofluids. Mohamad[14] examined the effect of nanofluid on heat transfer during forced and natural convection using the theories of classical physics and fluid mechanics. Mohamad[14] pointed out that it is not always true that nanofluid will enhance the heat transfer. Khanafer *et al.*[15] were the first to study buoyancy induced convective heat transfer for nanofluids numerically. They used a homogeneous model for predicting the heat transfer characteristic of the Cu/water nanofluids in the vertical square enclosure. They found that the Nusselt number (ratio of total heat transfer to convective heat transfer) increases by increasing the Grashof number (ratio of buoyancy force to viscous force). Also this increase in heat transfer was greater for higher volume fractions ($\phi$). Kim *et al.*[16] studied the convective instability driven by the buoyant force and heat transfer in nanofluids. They reported that convection in nanofluids was easily set up and the heat transfer coefficient enhances by all parameters considered during the investigation. Ho *et al.*[17] investigated the effect of using different models for effective thermal conductivity and dynamic viscosity in natural convection heat transfer. They concluded that using two different models in their numerical investigation lead to contradictory results while calculating convective heat transfer. Santra *et al.*[18] studied buoyancy induced heat transfer using Cu/water nanofluids with a varying volume fraction of $0 \le \phi \le 5.0\%$ and a Rayleigh number of $10^4 \le Ra \le 10^7$. They assumed nanofluids as non-Newtonian and used the Ostwald-de Waele model for calculating shear stress. They observed considerable deterioration in the heat transfer with an increase in the volume fraction of nanoparticles.

Hwang *et al.*[19] investigated buoyancy induced convective heat transfer in a rectangular cavity heated from below with $Al_2O_3$/water nanosuspension. They studied the effect of variance of volume fraction, particle diameter, and average temperature difference on the natural convection instability and heat transfer characteristics of nanofluids. They reported that the instability of $Al_2O_3$/water nanofluid with increase in volume fraction, decrease in particle size, and increase in average temperature becomes less than the corresponding basefluid. Deterioration in heat transfer coefficient was observed with the increase in size of nanoparticles and decrease in the average

[a]Author to whom correspondence should be addressed: pallab@iitm.ac.in

temperature. Tzou[20] studied the thermal instabilities in natural convection by performing the non-dimensional analysis. He obtained the close form of an equation from the method of eigenfunction expansion and weighted residual. He concluded that the critical Rayleigh number for nanofluids was one or two orders of magnitude lower than the basefluid owing to the Brownian and thermophoresis effects. Celli[21] investigated side heated 2D square cavity filled with nanofluids. For studying the behavior of nanofluids, a non-homogeneous model was taken into account. Numerical solution to the problem was obtained by means of a Galerkin finite element method. The thermophysical properties of the nanofluids were taken to be a function of the average volume fraction of nanoparticles dispersed inside the cavity. The average Nusselt number at the vertical walls was found to be sensitive for both the average volume fractions of the nanoparticles and also to the manner by which thermophysical properties were defined. They concluded that at optimal loading of nanoparticles the heat transfer performance shows peak which further increases with the magnification of their chosen controlling parameters. Avramenko *et al.*[22] studied the transport of heat, momentum, and concentration in a boundary layer of a nanofluid near a flat wall using Buongiorno's model. They concluded that with increases in the concentration of a nanofluid heat and momentum transfer intensifies. Also, they observed that neglecting local distribution of nanoparticle concentration had no effect on prediction of flow parameters. Choi *et al.*[23] investigated the effect of CuO/water nanofluids in laminar natural convection with both homogeneous and non-homogeneous models. They showed that both models predict the deterioration in the Nusselt number with volume fractions. They attributed the contradicting results between the experimental and numerical studies to the manner in which the Nusselt number was defined. Savithiri *et al.*[24] performed a numerical study by lattice Boltzmann study using a single component non-homogeneous model (SCNHM) for $Al_2O_3$/water nanofluid. They considered Brownian and thermophoresis as the important slip mechanisms and found that the heat transfer decreases with increase in volume fraction. They obtained a close agreement with the experimental values at higher volume fractions and proposed that the slip mechanism such as drag should also be considered for predicting the Nusselt number. They also concluded that inclusion of Brownian and thermophoretic diffusion results in increasing thermal diffusion which reduces the convective transport of heat.

Qi *et al.*[25] developed a two-phase Lattice Boltzmann model for natural convection in nanofluids for $Ra = 10^3$ and $Ra = 10^5$. They considered all the interactive forces (gravity and buoyancy force, drag force, interaction potential force, and Brownian force) existing between the nanoparticles and the basefluid. The effects of different nanoparticle volume fractions and Rayleigh numbers which are products of the Grashof and Prandtl numbers (the Prandtl number is a ratio of momentum diffusivity to thermal diffusivity) on natural convection heat transfer of prepared from $Al_2O_3$ nanoparticles were investigated. They have seen that the average Nusselt number of the enclosure increases with increasing volume fraction of the nanoparticles and this rate is even higher at high Ra. They also found that Brownian, interaction potential, and gravity-buoyancy force had incremental effects on natural convective heat transfer, while drag force had a decremental effect. Besides, the effects of various forces on nanoparticle volume fraction distribution in the square enclosure were also studied. They reported that the driving force because of the temperature difference has the highest effect on the volume fraction distribution of nanoparticles. Savithiri *et al.*[26] studied the multi-component non-homogeneous model (MCNHM) using lattice Boltzmann simulation. They performed the scaling analysis to confirm the dominance of various forces in capturing the flow physics and heat transfer in natural convection. The effect of all slip forces was studied individually and it was concluded that drag is the most important slip mechanism for accurately predicting the heat transfer at higher volume fractions.

Most of the experimental studies pertaining to buoyancy induced convective heat transfer are performed using spherical type of nanoparticles and all of them have reported deterioration in the Nusselt number. To the best of the author's knowledge, this is the first effort in which experiments and numerical modeling have been performed for non-spherical nanoparticles such as MWCNT (Multi-Walled Carbon Nanotube) (tubular shape) and graphene (flake shape) and compared it with the spherical nanoparticles ($Al_2O_3$). In order to study the heat transfer characteristics and to investigate the role of slip mechanisms in natural convection, a thorough numerical study is conducted. A numerical investigation is done at various Rayleigh numbers and volume fractions using three models, namely, SCHM (Single Component Homogeneous Model), SCNHM (Single Component Non-Homogeneous Model), and MCNHM (Multi-Component Non-Homogeneous Model). SCHM and SCNHM are modeled using the OpenFOAM (Open source Field Operation And Manipulation) code, while for implementation of MCNHM, Ansys-Fluent is used as a computational fluid dynamics (CFD) tool. Comparison of the numerical and experimental results is done for above mentioned nanofluids. Finally, drawbacks and applicability of each of the model are explained based on the comparison.

## II. EXPERIMENTAL METHODOLOGY

### A. Nanofluids preparation

A two-step method is used for preparing the $Al_2O_3$/water and MWCNT/water nanofluids. $Al_2O_3$ nanoparticles (Nanoshel, high purity 99.5%, 80 nm) of density of 3950 kg/m$^3$ are mixed in required quantity with distilled water to prepare $Al_2O_3$/water nanofluids. Similarly, MWCNT nanoparticles (Nanoshel, OD 10–20 nm, length 3–8 $\mu$m) with density of 2000 kg/m$^3$ are used for preparing the MWCNT/water nanofluids. A probe sonicator (QSonica) is used to sonicate the mixtures for 15 min. A small quantity of SDS (Sodium Dodecyl Sulphate) is added with the nanofluids to increase the stability of the suspension. Prepared nanofluids were stable for about two days. A single-step process is used to prepare the graphene/water nanofluids. First, Hummer's method is used to prepare the graphene-oxide suspension and then the sulphonation method is carried out to extract graphene from

graphene-oxide. More details about the nanofluid preparation can be found in Ref. 13.

### B. Experimental results and discussion

The present section shows the experimental results of the natural convection in a differentially heated cavity filled with three types of nanosuspensions at different volume fractions. Nusselt numbers plotted in all the figures are averaged Nusselt numbers. Some of the important results from the experimental investigation are plotted in Fig. 1. The values of the normalized Nusselt number which is the ratio of non-dimensional temperature gradient of nanofluid to non-dimensional temperature gradient of basefluid ($Nu_{norm} = Nu_{nf}/Nu_{bf}$) for all three nanofluids at volume fractions of 0.1% and 0.5% are shown in Fig. 1, respectively. Here, subscripts "*bf*" and "*nf*" indicate properties related to basefluid and nanofluid, respectively. It can be seen from Fig. 1 that alumina/water nanosuspensions show deterioration in heat transfer at all the volume fractions and it further deteriorates with increase in volume fraction. For a Rayleigh number ($Ra$) of $1 \times 10^6$, with MWCNT/water nanofluid, an enhancement of about 35%–20% is observed at the volume fraction of 0.1% and 0.3%, respectively. However, further increasing the volume fraction to 0.5% has shown deterioration. Similar to MWCNT/water nanosuspensions, graphene/water nanosuspensions show enhancement at a volume fraction of 0.1% which is about 20%. But for the volume fractions of 0.3% and above, graphene/water nanosuspension shows reduction in the Nusselt number ($Nu$). At a volume fraction of 0.5% and a Rayleigh number of $1 \times 10^6$ as seen in Fig. 1, deterioration of about 6%, 4%, and 15% is observed for alumina/water, MWCNT/water, and graphene/water nanosuspensions, respectively. The detailed description of the experimental setup, methodology, and results is given in the work of Joshi and Pattamatta.[13]

Therefore, it can be inferred from the experimental results that there is enhancement in heat transfer for non-spherical particles at lower volume fractions, while deterioration in the Nusselt number is observed at higher volume fractions for all types of nanosuspensions. The underlying physics for the enhancement or deterioration observed experimentally cannot be simply attributed to relative changes in the thermophysical properties alone. It seems that slip mechanisms play a vital role, and to capture the exact effect of slip mechanisms, a numerical study is conducted. Numerical investigation is performed using three different models, namely, SCHM, SCNHM, and MCNHM with different volume fractions and Rayleigh numbers.

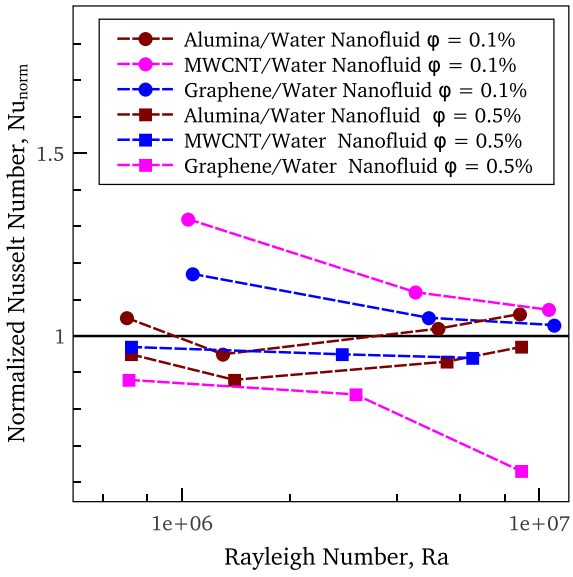


FIG. 1. Variation of the normalized Nusselt number with the Rayleigh number at 0.1% and 0.5% of volume fractions.

### C. Models for thermophysical properties

Thermophysical properties of nanofluids such as effective viscosity [$\mu$ (Pa s)] and thermal conductivity [$k$ (W/mK)] are measured in-house. Thermal conductivity is measured with the KD2 pro Decagon thermal analyzer based on the principle of the transient hot wire method. The uncertainty in the measurement of thermal conductivity is about 1.2%. Thermal conductivity of MWCNT (Multi-Walled Carbon Nanotube)/water and graphene/water nanofluids is measured for the given temperature and volume fractions. Figure 2(a) shows the trend line of effective thermal conductivity of nanofluids with varying volume fractions. Dynamic viscosity of the nanofluids is measured with an automated microviscometer (Anton Paar GmbH, Austria) using the rolling ball method and the uncertainty in the measurement is about 1.0%. Similarly, the dynamic viscosity of MWCNT/water nanofluid and graphene/water is measured for the given temperature and volume fractions. It is observed from Fig. 2(b) that the dynamic viscosity of MWCNT/water is the highest while it is lowest for alumina/water nanofluid. All the thermophysical properties mentioned in Fig. 1 are averaged properties.

The quadratic equation obtained from curve fitting the data for thermal conductivity and viscosity from the experimental measurement for the considered nanofluids is stated in the following equations:

1. Alumina/water nanofluid:

$$k_{nf} = k_{bf}(1 + 2.136\phi + 45.021\phi^2), \quad (1)$$

$$\mu_{nf} = \mu_{bf}(1 + 4.363\phi + 308.81\phi^2). \quad (2)$$

2. MWCNT/water nanofluid:

$$k_{nf} = k_{bf}(1 + 43.43\phi - 1702\phi^2), \quad (3)$$

$$\mu_{nf} = \mu_{bf}(1 + 113.4\phi + 7735\phi^2). \quad (4)$$

3. Graphene/water nanofluid:

$$k_{nf} = k_{bf}(1 + 48.45\phi + 3896.2\phi^2), \quad (5)$$

$$\mu_{nf} = \mu_{bf}(1 + 31.44\phi + 10992.4\phi^2). \quad (6)$$

In order to investigate the rheological properties for each of the prepared nanosuspensions, a test using the rotational type rheometer is performed at three different volume fractions ($\phi$ = 0.1%, 0.3%, and 0.5%). It can be clearly seen from Fig. 2(c) that at a given range of volume fraction and shear rate, alumina/water and MWCNT/water nanofluids impart Newtonian behavior as viscosity is constant for

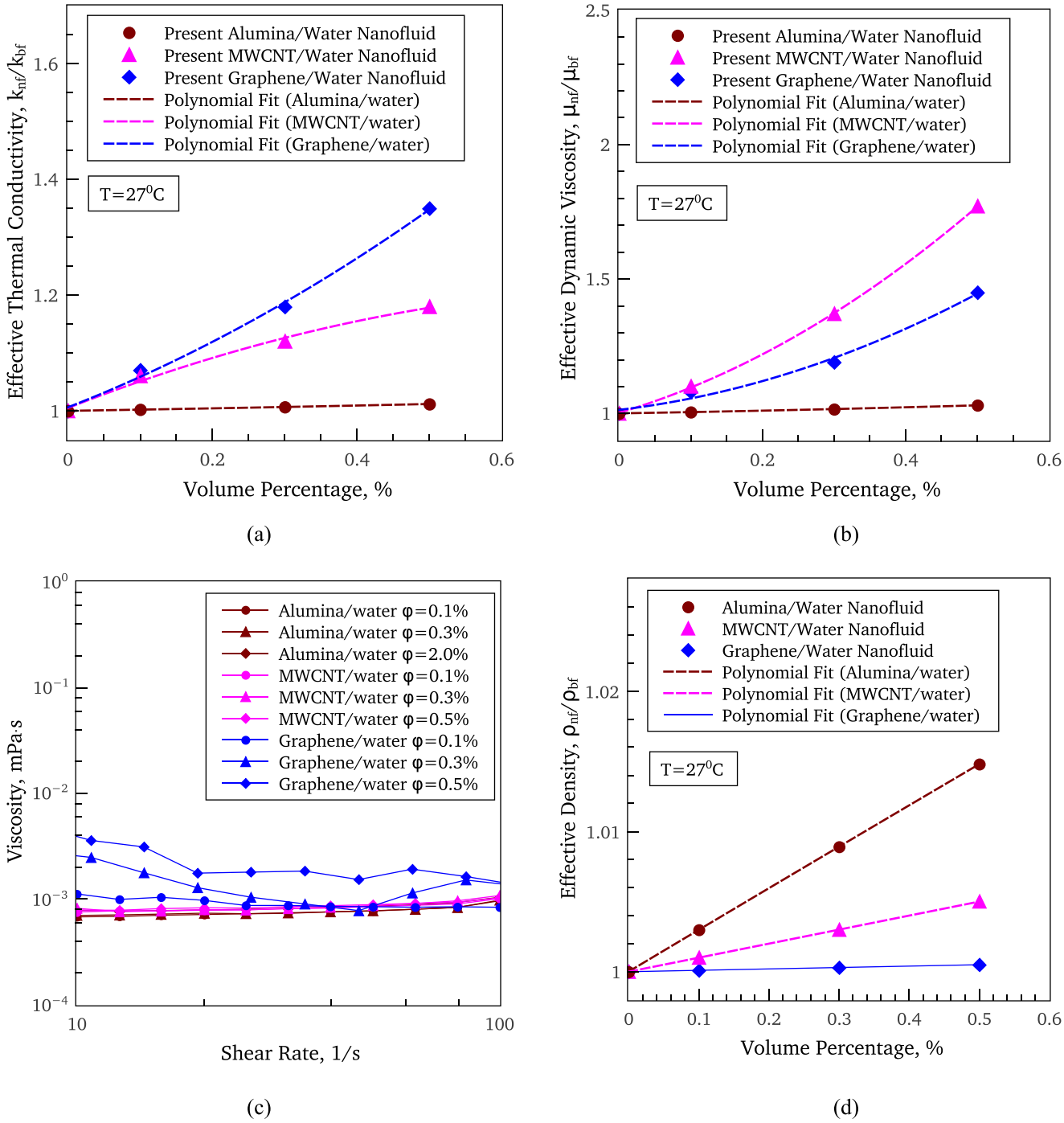


FIG. 2. Variation of (a) effective thermal conductivity, (b) effective dynamic viscosity, (c) dependence of dynamic viscosity to shear rate, and (d) effective density of nanofluids at different volume fractions.

the given range of shear rate. Whereas, graphene/water nanofluid starts showing slight shear thinning from a volume fraction of 0.3% and therefore maximum volume fractions is restricted to 0.5% for both experimental and numerical analyses.

Other thermo-physical properties such as specific heat [$c_p$ (J/kgK)] formulated by Ref. 27 and the density [$\rho$ (kg/m$^3$)] and volumetric thermal expansion coefficient [$\beta$ (1/K)] calculated based on the Maxwellian equation are, respectively, given by

$$\rho_{nf} c_{p,nf} = \phi \cdot \rho_{np} \cdot c_{p,np} + (1-\phi) \cdot \rho_{bf} \cdot c_{p,bf}, \quad (7)$$

$$\rho_{nf} = \phi \cdot \rho_{np} + (1-\phi) \cdot \rho_{bf}, \quad (8)$$

$$\beta_{nf} = \phi \cdot \beta_{np} + (1-\phi) \cdot \beta_{bf}, \quad (9)$$

where subscript "*np*" indicates properties related to nanoparticles. The specific heat, density, and volumetric thermal expansion of the alumina, MWCNT, and graphene nanoparticles are obtained from the literature[28–31] and are shown in Table I. The values of effective density for the nanofluids are compared in Fig. 2(d).

TABLE I. Thermophysical properties of nanofluid.

| Types of nanoparticles | Specific heat capacity (J/kg K) | Density (kg/m$^3$) | Volumetric thermal expansion coefficient (1/K) |
|---|---|---|---|
| Alumina | 765 | 3950 | $8.5 \times 10^{-4}$ |
| MWCNT | 710 | 2000 | $2.1 \times 10^{-5}$ |
| Graphene | 710 | 1100 | $-5.0 \times 10^{-6}$ |

## III. PROBLEM DEFINITION AND NUMERICAL METHODOLOGY

The computational domain used in the present study is shown in Fig. 3. The left-side wall is maintained at a higher temperature and the right-side wall is maintained at a lower temperature. The top and bottom walls are maintained at the adiabatic boundary condition. Numerical studies are performed using three different models: SCHM, SCNHM, and MCNHM.

### A. Single component homogeneous model (SCHM)

Single component homogeneous models consider basefluid (de-ionized water) and nanoparticles as an effective matrix and thus effective properties are directly plugged into the governing equations. The concentration of nanoparticles is uniform throughout the domain and also remains constant with time.

The governing equations for the specified natural convection problem are as follows: Continuity equation for the nanofluid:

$$\nabla \cdot u = 0. \tag{10}$$

Momentum equation for the nanofluid:

$$\rho_{nf}\left(\frac{\partial u}{\partial t} + u \cdot \nabla u\right) = -\nabla p + \nabla \cdot \left(\mu_{nf}\left[\nabla u + \nabla u^t\right]\right) + \rho_{nf} g \beta_{nf} \triangle T, \tag{11}$$

where $\nabla u^t$ is the transpose of $\nabla u$ and the energy equation for nanofluids is

$$\left(\frac{\partial T}{\partial t} + u \cdot \nabla T\right) = \alpha_{nf} \nabla^2 T, \tag{12}$$

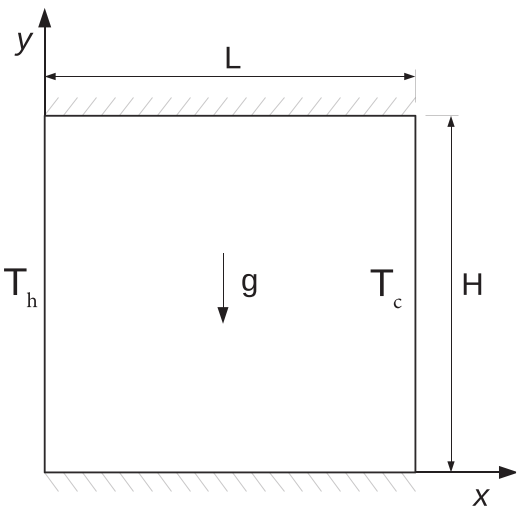


FIG. 3. Schematic of computational domain.

where

$$\alpha_{nf} = \frac{k_{nf}}{(\rho c_p)_{nf}}, Nu_{loc} = -\frac{\partial \theta}{\partial y}, \theta = \frac{T - T_c}{T_h - T_c},$$

where subscripts "$c$" and "$h$" indicate properties pertaining to cold and hot wall, respectively. The average Nusselt number is given by

$$Nu_{avg} = \frac{1}{H}\int_0^H Nu_{loc} dx, \tag{13}$$

where "$H$" is the characteristic dimension in meters and "$T$" is the temperature in Kelvin. The boundary condition for the specified problem in the mathematical form is represented as follows:

$$u = v = T = 0 \quad for \quad t = 0, \tag{14}$$

$$u = v = \frac{\partial T}{\partial y} = 0 \quad at \quad y = 0, H \quad and \quad 0 \le x \le L, \tag{15}$$

$$T = T_h, \quad u = v = 0 \quad at \quad x = 0, \quad 0 \le y \le H, \tag{16}$$

$$T = T_c, \quad u = v = 0 \quad at \quad x = L, \quad 0 \le y \le H. \tag{17}$$

The following assumptions are made while solving the governing equations:

- The fluid is incompressible, Newtonian, and laminar.
- The Boussinesq approximation is valid.
- Basefluid molecule and nanoparticles are in thermal equilibrium and there is no slip between them.

The effective properties such as specific heat, density, and thermal expansion coefficient are calculated from Eqs. (7)–(9) at a given temperature and volume fraction. The quadratic equation for the thermal conductivity and the viscosity for specific nanofluids given in Eqs. (1)–(6) are incorporated into the present model.

The governing equations with the specified boundary conditions are solved using the finite volume method. OpenFOAM, an open source computational fluid dynamics tool, is used for simulating this model.[32] The PIMPLE algorithm, which is a blend of PISO (Pressure Implicit with Split Operator) and SIMPLE (Semi-Implicit Method for Pressure Linked Equation) algorithms, is used for solving the governing equations.

### B. Single component non-homogeneous model (SCNHM)

The assumptions made while solving the governing equations for the single component non-homogeneous model are same as that of the homogeneous model with an exception that the Brownian and thermophoresis are considered as the prominent slip mechanisms.

The governing equations for SCNHM are referred from Buongiorno's[33] model. In this model along with the momentum equation for the nanosuspensions, a separate diffusion equation for the nanoparticles is also solved. The energy equation is modified by including Brownian and thermophoretic diffusion terms. The conservation equation for continuity and momentum is identical to that of SCHM, while the diffusion and modified energy equation for the nanosuspensions are given as follows:

The advective diffusion equation for the nanoparticles is

$$\frac{\partial \phi}{\partial t} + u \cdot \nabla \phi = \nabla \cdot \left( D_B \nabla \phi + D_T \frac{\nabla T}{T} \right), \tag{18}$$

where $D_B$ and $D_T$ are Brownian and thermophoretic diffusion terms and are given by

$$D_B = \frac{K_B T}{3\pi \mu_{nf} d_p}, \tag{19}$$

$$D_T = 0.26 \frac{k_{bf}}{2k_{bf} + k_p} \frac{\mu_{nf}}{\rho_{nf}} \phi, \tag{20}$$

and the energy equation for nanofluids is

$$\begin{aligned}(\rho C_p)_{nf} \left( \frac{\partial T}{\partial t} + u \cdot \nabla T \right) &= \nabla \cdot (k \nabla T) \\ &+ \rho_p C_{p_p} \left( D_B \nabla \phi \cdot \nabla T + D_T \frac{\nabla T \cdot \nabla T}{T} \right).\end{aligned} \tag{21}$$

For specifying the volume fraction at the wall, the zero flux boundary condition is imposed at the wall given by

$$\left( \left[ -\rho_p D_B \nabla \phi - \rho_p D_T \frac{\nabla T}{T} \right] \cdot \vec{n} \right)_w = 0. \tag{22}$$

The fluxes due to Brownian and thermophoretic coefficient diffusion are determined by the following equation:

$$j_{loc_B} = -\frac{\rho_{nf} C_{p_p}}{k_{nf}} \left( D_B \frac{\partial \phi}{\partial y} \right), \tag{23}$$

$$j_{loc_T} = -\frac{\rho_{nf} C_{p_p}}{k_{nf}} \left( D_T \frac{\partial \phi}{\partial y} \right). \tag{24}$$

The average fluxes are calculated as

$$j_{avg_B} = \frac{1}{H} \int_0^H j_{loc_B} dx, \tag{25}$$

$$j_{avg_T} = \frac{1}{H} \int_0^H j_{loc_T} dx. \tag{26}$$

Thus the local non-dimensional temperature gradient is represented as

$$Nu_{loc} = -\frac{\partial \theta}{\partial y} - (j_{loc_B} + j_{loc_T}). \tag{27}$$

In SCNHM, the flow physics is affected by the Brownian and thermophoretic diffusion and it changes the flow field thereby changing the heat transfer characteristics. This model is also implemented in OpenFOAM by modifying the volume fraction boundary condition as stated above. In the case of SCNHM, all the effective properties are calculated based on the given volume fraction and they alter as the solution progresses depending on the concentration gradient and thus cause non-uniformity.

### C. Multi-component non-homogeneous model (MCNHM)

In this model, all the slip mechanisms are taken into consideration and are based on the Lagrangian approach. The slip forces taken into consideration are Brownian, thermophoresis, drag, lift, rotational, magnus, and gravity. MCNHM is modeled using the finite volume method, and Ansys-Fluent is used as the computational tool. In the Ansys-Fluent, DPM (Discrete Phase Model)[34] which is based on the Lagrangian method is adapted for the present simulations. Particle trajectory is predicted by integrating all the forces and equating it with the particle inertia. The equation for motion of the particle is written as

$$\frac{du_p}{dx} = F_D(u - u_p) + \frac{g_x(\rho_p - \rho)}{\rho_p} + \sum F_x, \tag{28}$$

where "$u$" is the velocity of the fluid phase and "$u_p$" is the velocity of the particle. The other forces in force balance "$F_x$" are as follows:

$$\sum F_x = F_B + F_T + F_M + F_L + F_R. \tag{29}$$

Equation for the basefluid by including the source term is given by

$$\begin{aligned}\rho_{nf} \left( \frac{\partial u}{\partial t} + u \cdot \nabla u \right) &= -\nabla p + \nabla \cdot \left( \mu_{nf} \left[ \nabla u + \nabla u^t \right] \right) \\ &+ \rho_{nf} g \beta_{nf} \triangle T - S_{np},\end{aligned} \tag{30}$$

where "$S_{np}$" is the source term which incorporates the effects due to the presence of all slip mechanisms. $F_B$ is the Brownian force generated by the random motion of the nanoparticles within the basefluid. $F_T$ is the thermophoretic force generated on the suspended nanoparticles due to the temperature gradient. $F_M$ is the force caused due to the Magnus effect. $F_L$ is the lift force generated on free rotating particle in a shear flow. $F_R$ is a force experienced by the particle due to rotational motion about the fixed axis. A detailed explanation for each of the slip force is mentioned in the literature.[26] For the present study, particles are injected from the interior surface of the cavity uniformly. The number of particles to be injected is calculated based on the volume fraction of the nanoparticles and the diameter of the nanoparticles considered in the present study. The number of particles is adjusted from the number of parcels in the transient solver. The drag force is modeled for alumina nanoparticles using the Stokes-Cunningham drag law,[34] while for MWCNT and graphene nanoparticles, a non-spherical drag law is used by specifying sphericity considering the shape effects. Thermal properties mentioned in Table I are incorporated in the model.

TABLE II. Inputs to the solver for MCNHM.

| Nanofluid Nanofluid | Diameter (nm) | Shape factor | Volume fraction (%) | Number of particles |
|---|---|---|---|---|
| Alumina | 80 | 1 | 0.1 | $3.18 \times 10^8$ |
| | | | 0.3 | $9.55 \times 10^8$ |
| | | | 0.5 | $1.59 \times 10^9$ |
| | | | 0.75 | $2.39 \times 10^9$ |
| | | | 1.0 | $3.18 \times 10^9$ |
| | | | 2.0 | $6.37 \times 10^9$ |
| MWCNT | 114 | 5 | 0.1 | $1.56 \times 10^8$ |
| | | | 0.3 | $4.67 \times 10^8$ |
| | | | 0.5 | $7.78 \times 10^8$ |
| Graphene | 80 | 5 | 0.1 | $3.15 \times 10^8$ |
| | | | 0.3 | $9.44 \times 10^8$ |
| | | | 0.5 | $1.57 \times 10^9$ |

The maximum number of time steps is specified as 100000. The PISO algorithm is used to solve the MCNHM cases. For checking the convergence, variation in the values of the Nusselt number, isotherms, and streamlines is continuously monitored. Nusselt number values at the wall are calculated by defining a user defined function. The method of solving the equation in DPM is specified by Bianco *et al.*[35] In Table II, the input parameters for the MCNHM model, such as diameter, shape factor, volume fraction, and number of particles, are mentioned.

## IV. GRID INDEPENDENCE AND SOLVER VALIDATION

For numerical analysis, initially grid independence study is performed. The grid size is varied from 200 × 200 to 600 × 600 with a step size of 50 in both $x$ and $y$ directions. It is seen from the grid independence study that for a grid size of 550 × 550, the deviation in the Nusselt number is found to be less than 1%. The variation of the heat flux at the left wall and the velocity at the mid-section of the cavity with different grid sizes are shown in Figs. 4(a) and 4(b), respectively. Therefore

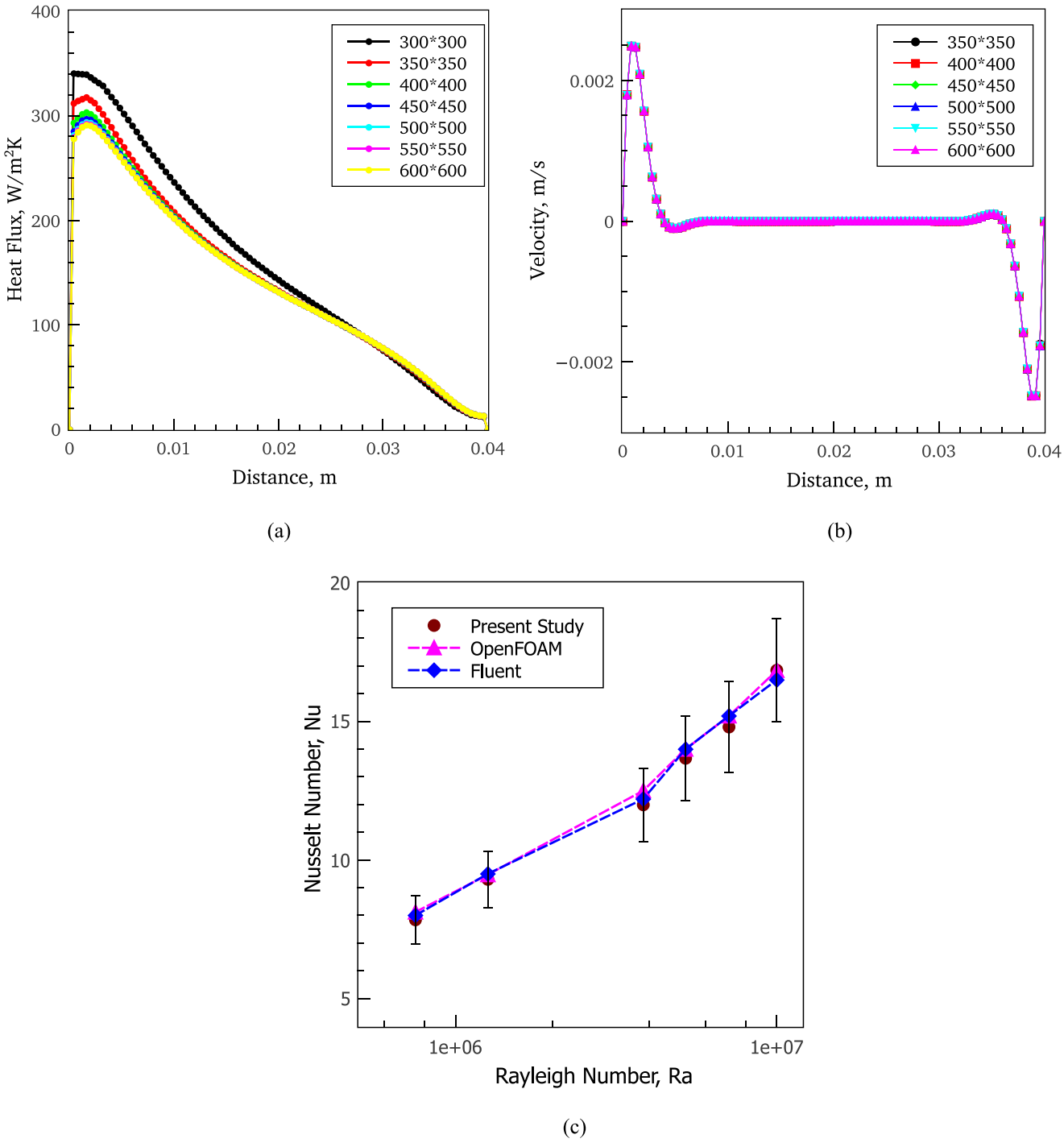


FIG. 4. (a) Heat flux calculated at the left wall. (b) Velocity at the mid-section of the cavity for various grid sizes. (c) Variation of the Nusselt number with the Rayleigh number for basefluid.

for computational efficiency, a 550 × 550 grid is used for all the studies.

To validate the numerical solvers, that is, OpenFOAM and Ansys-Fluent, simulations are conducted for basefluid (de-ionized water) for different Rayleigh numbers ranging from $7 \times 10^5$ to $1 \times 10^7$ and are compared with present experimental data [see Fig. 4(c)]. It can be observed from Fig. 4(c) that the simulated results from both solvers are found to be

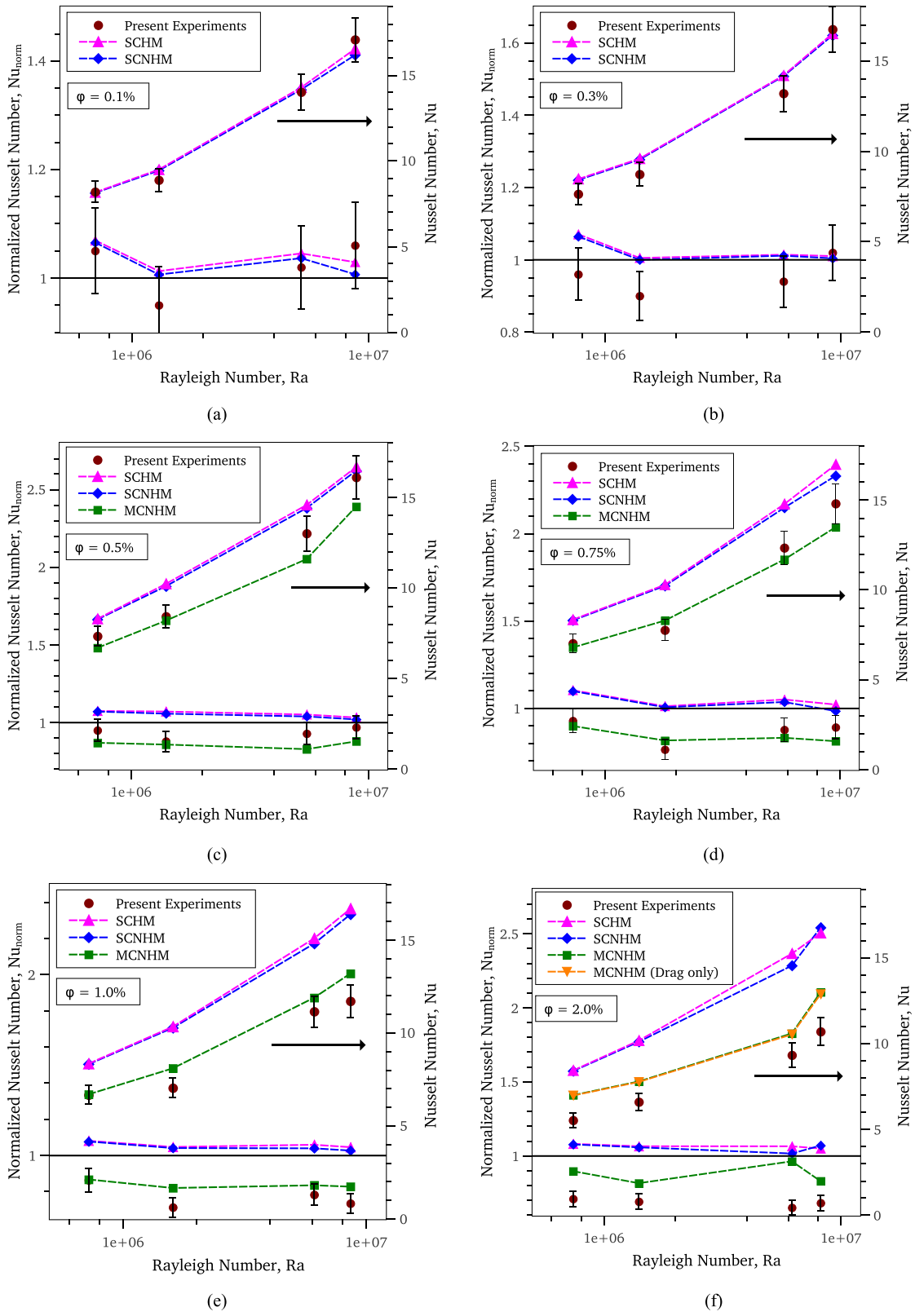


FIG. 5. Comparison of experimental and numerical results of alumina/water nanofluid at (a) 0.1%, (b) 0.3%, (c) 0.5%, (d) 0.75%, (e) 1.0%, and (f) 2.0% of volume fraction.

in good agreement with the present experimental values of the Nusselt number for the basefluid. Further numerical studies are done for alumina/water with varying volume fractions of 0.1%, 0.3%, 0.5%, 0.75%, 1.0%, and 2.0%. For MWCNT/water and graphene/water nanofluids, the studies are carried out with volume fractions of 0.1%, 0.3%, and 0.5%.

## V. RESULTS AND DISCUSSION

### A. Comparison of models for particle based nanosuspension (alumina/water)

For alumina/water nanofluid, experiments are carried out for 0.1%, 0.3%, 0.5%, 0.75%, 1.0%, and 2.0% of volume fractions. At lower volume fractions, the Nusselt number values are slightly above the corresponding basefluid values as seen in Fig. 5(a), but this enhancement is within the experimental uncertainty. At higher volume fractions of about 1.0% [Fig. 5(e)] and 2.0% [Fig. 5(f)], significant deterioration up to 40% is observed in the heat transfer. This signifies that addition of alumina nanoparticles to the basefluid deteriorates heat transfer at all volume fractions. To understand the flow physics and heat transfer characteristics, different models are used to mimic the experiments and then the results are compared.

Figure 5 shows the variation of two quantities; first the variation of a Nusselt number at the top which is quantified on the secondary y-axis and second the variation of a normalized Nusselt number at the bottom which is quantified on the primary *y-axis* with respect to the Rayleigh number. At a volume fraction of 0.1%, both SCHM and SCNHM are in close agreement with experimental results for all ranges of Rayleigh numbers as shown in Fig. 5(a). Figure 5(a) also shows that both SCHM and SCNHM predict almost same values of the Nusselt number and there is only slight variation between these models for higher Rayleigh numbers. A same trend is observed for a volume fraction of 0.3% as seen in Fig. 5(b). However, as the volume fraction increases over 0.5%, that is, for 0.75%, 1.0%, and 2.0% shown in Figs. 5(d)–5(f), respectively, SCHM and SCNHM start deviating from the experimental observations. Thus, consideration of merely effective properties in SCHM and inclusion of Brownian and thermophoresis forces in SCNHM are not sufficient enough to predict the deterioration at higher volume fractions. Therefore the numerical study using MCNHM which incorporates all the slip forces seems to be important.

It can seen from Fig. 5(c) that the SCHM and SCNHM start over-predicting experimental values and MCNHM which includes all the slip forces mentioned earlier is found to be the closest among all the models considered. As the volume fraction increases, the importance of drag-based slip forces increases. In MCNHM, all mechanisms such as Brownian, thermophoresis, drag forces, rotational, magnus, and lift are taken into consideration. For a Rayleigh number of $1 \times 10^7$ and a volume fraction of 2.0%, the difference in the Nusselt number when compared with experiments is about 45% and 40% for SCHM and SCNHM, respectively. However for MCNHM, the deviation difference is only about 15% when compared to experimental values which can be clearly seen in Fig. 5(f). Figure 5(f) also shows the variation of the Nusselt number considering the drag force and neglecting all other forces. It is clearly seen that removing other slip forces does not show any effect on the Nusselt number values and therefore we can conclude that drag-based slip force becomes the most predominant force at higher volume fractions for the spherical type of nanosuspensions.

### B. Comparison of isotherms and streamlines of different models for alumina/water nanofluid

As different numerical models are considered in the present study which accounts for different slip mechanisms, both the flow field and temperatures patterns would vary accordingly. In this section, changes in the isotherms and streamlines inside the cavity with different models are discussed for alumina/water nanofluid at a volume fraction of 2.0% and a Rayleigh number of $8.2 \times 10^6$. All the results are compared with the basefluid at the same Rayleigh number. A similar study can be extended to other types of nanosuspensions such as MWCNT/water and graphene/water.

Figures 6(a), 6(c), and 6(e) represent the comparison of isotherms for different models with respect to the basefluid. It can be seen from Figs. 6(a) and 6(c) that there is a minor shift in the isotherms which indicates a slight change in

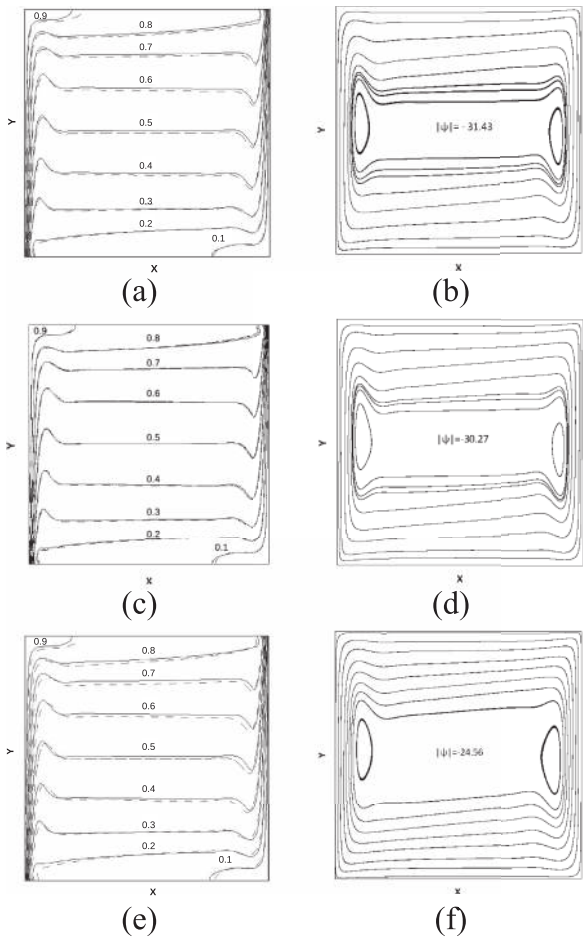


FIG. 6. Comparison of (a) isotherm (solid line—basefluid and dotted line—SCHM), (b) streamlines for SCHM, (c) isotherm (solid line—basefluid and dotted line—SCNHM), (d) streamlines for SCNHM, (e) isotherm (solid line—basefluid and dotted line—MCNHM), (f) streamlines for MCNHM.

temperature gradient for SCHM and SCNHM when compared with the basefluid. Isotherms for MCNHM when compared to the other two models and the basefluid show more shift as is seen in Fig. 6(e) which means the heat transport is least in this case which in turn gives a lower value of the Nusselt number.

Streamlines indicate the flow direction of the fluid inside a cavity. Streamlines are circulated vortices, the direction of which is represented by an arrow in the present case. Streamlines for three models, namely, SCHM, SCNHM, and MCNHM, are plotted in Figs. 6(b), 6(d), and 6(f), respectively. It can be inferred from Figs. 6(b) and 6(d) that streamlines from SCHM and SCNHM models are almost similar to the basefluid. Whereas as shown in Fig. 6(f), for MCNHM it is observed that due the inclusion of the slip forces, there is more resistance to flow and the advective motion of nanofluids reduces compared with that of basefluid.

### C. Comparison of models for tubular based nanosuspension (MWCNT/water)

For tubular based nanosuspension (MWCNT/water), experiments are performed at 0.1%, 0.3%, and 0.5% of volume fractions. As stated in the experimental study, the enhancement in the Nusselt number is observed for lower volume fractions of 0.1% and 0.3% for MWCNT/water nanosuspension, while for the volume fraction of 0.5%, deterioration is seen. In order to study the effect of all the slip forces and the possible mechanisms for enhancement, numerical investigation is carried out in the present study. It should be noted that despite the different nanoparticle size and nanoparticle effective thermal conductivity, the streamlines and isotherm patterns of MWCNT/water nanofluids are similar to that of the alumina/water nanofluids shown in Fig. 6.

Figure 7 shows the variation in the Nusselt number and the normalized Nusselt number for different Rayleigh numbers. It is seen in Figs. 7(a) and 7(b) that SCHM and SCNHM are closer to the experimental results at volume fractions of 0.1% and 0.3% but cannot capture the enhancement observed quantitatively. While MCNHM shows deterioration at all volume fractions considered in the present study, this can be attributed to the inclusion of the drag force which opposes the flow and causes deterioration. The difference in the Nusselt number for a volume fraction of 0.1% using SCHM, SCNHM, and MCNHM as compared with experiments is about 12%, 12%, and 20%, respectively. At a higher volume fraction of 0.5% as seen from Fig. 7(c), SCHM and SCNHM overpredict the experimental values, while MCNHM comes closer to the experiments. This is because at higher volume fractions, drag becomes an important slip mechanism and thus modeling drag accurately predicts the Nusselt number values. For tubular-based nanosuspensions, SCHM and SCNHM models are closer to the experimental values at lower volume fractions but cannot predict the enhancement quantitatively, while for higher volume fractions, MCNHM is in good agreement with the experiments due to inclusions of the drag force.

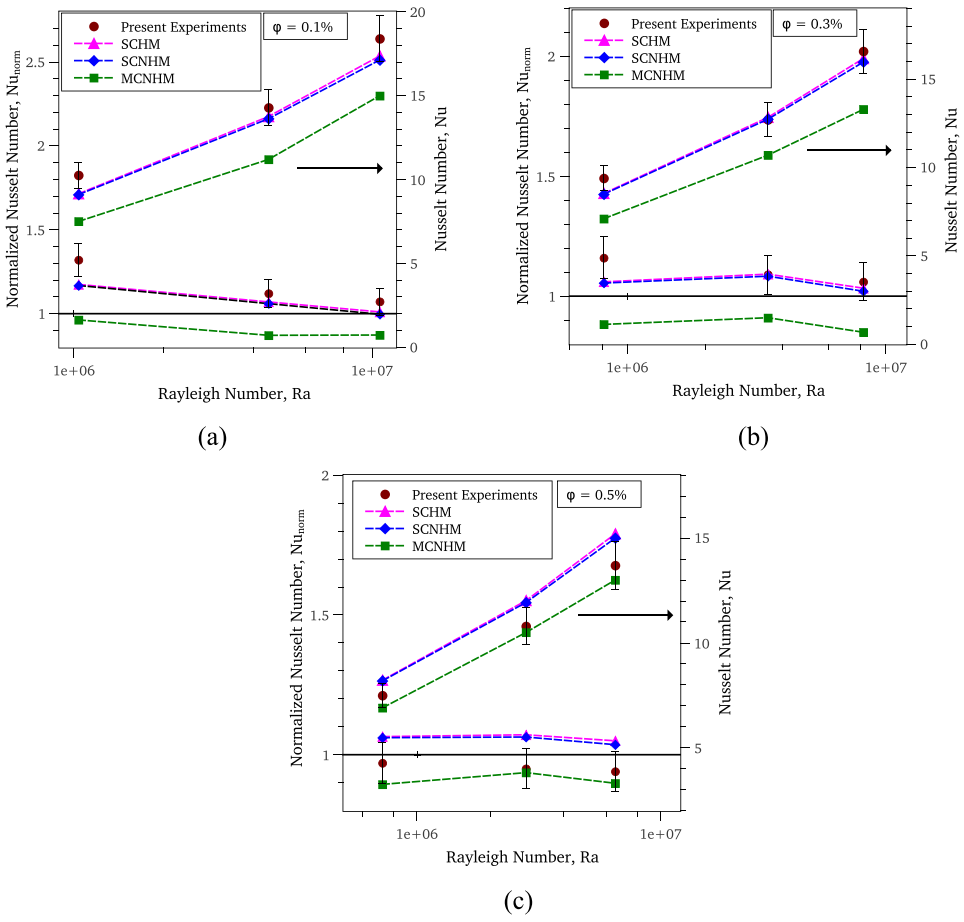


FIG. 7. Comparison of experimental and numerical results of MWCNT/water nanofluid at (a) 0.1%, (b) 0.3%, and (c) 0.5% of volume fraction.

### D. Comparison of models for flake based nanosuspension (graphene/water)

Experiments with graphene/water nanofluid are done with 0.1%, 0.3%, and 0.5% volume fractions. The normalized Nusselt number plots for graphene/water nanofluids are shown in Fig. 8. Experimentally, enhancement of about 20% is observed compared to the basefluid at a volume fraction of 0.1%, while there is deterioration in heat transfer at 0.3% and 0.5% volume fractions. A deterioration of about 40% is observed at 0.5% of the volume fraction and a Rayleigh number of $1 \times 10^7$. It should be noted that despite the different nanoparticle size and nanoparticle effective thermal conductivity, the streamlines and isotherm patterns of graphene/water nanofluids are identical to that of the alumina/water nanofluids shown in Fig. 6. Numerical results using all three models are investigated for the flake shape-based nanofluid and are presented below.

Variation of the Nusselt number with different Rayleigh numbers for graphene/water nanofluid is plotted in Fig. 8. At 0.1% of volume fraction, SCHM and SCNHM are able to predict the Nusselt number values qualitatively as seen in Fig. 8(a). At higher volume fractions of 0.3% and 0.5% as seen in Figs. 8(b) and 8(c), respectively, SCHM and SCNHM are quite off from the experimental observations, whereas MCNHM becomes closer to the experimental values. A similar argument stated for MWCNT/water nanofluid can be extended to explain this behavior, that is, as the volume fractions keep on increasing, the drag becomes dominant and buoyancy decreases thereby decreasing the heat transfer which can be modeled by MCNHM only. The percentage variation in Nusselt numbers at a volume fraction of 0.5% for a Rayleigh number of $1 \times 10^7$ as seen in Fig. 8(c) is 30%, 25%, and 15% for SCHM, SCNHM, and MCNHM, respectively.

### E. Possible mechanism for enhancement at lower volume fraction of non-spherical type nanosuspensions

It can be concluded from the comparison of experimental and numerical results that at lower volume fractions for these types of nanofluids, SCHM and SCNHM predict the Nusselt number values fairly well. While at higher volume fractions, as drag becomes important, slip mechanism MCNHM becomes closer to experimental results. The percentage deviation of the normalized Nusselt number with respect to basefluid values is plotted in Fig. 9. It is seen for Fig. 9 that SCHM and SCNHM always predict enhancement with respect to basefluid no matter which volume fraction or the type of nanofluid we are considering. Therefore, it is the inherent nature of these two models to show enhancement irrespective of the type of nanofluids. Also, it is seen that MCNHM always show deterioration for all types of nanofluids. This is because it considers all possible slip mechanisms that are present between particles and basefluid molecules. Thus it can be concluded that there is not a

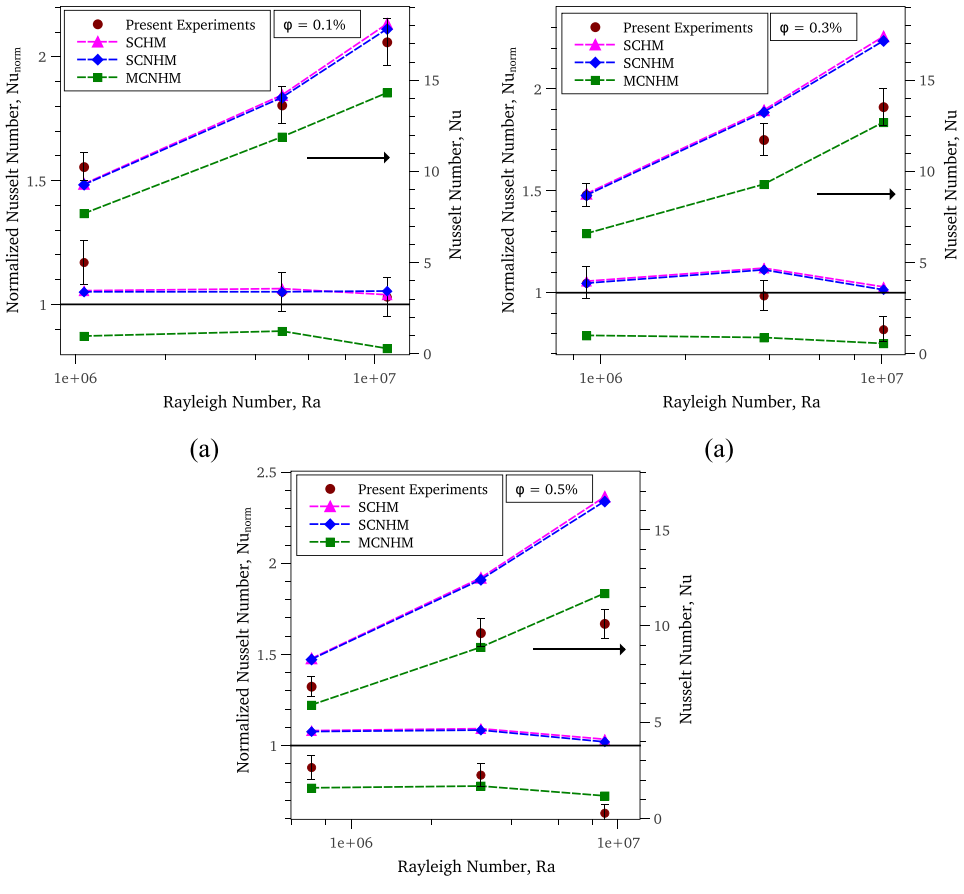


FIG. 8. Comparison of experimental and numerical results of graphene/water nanofluid at (a) 0.1%, (b) 0.3%, and (c) 0.5% of volume fraction.

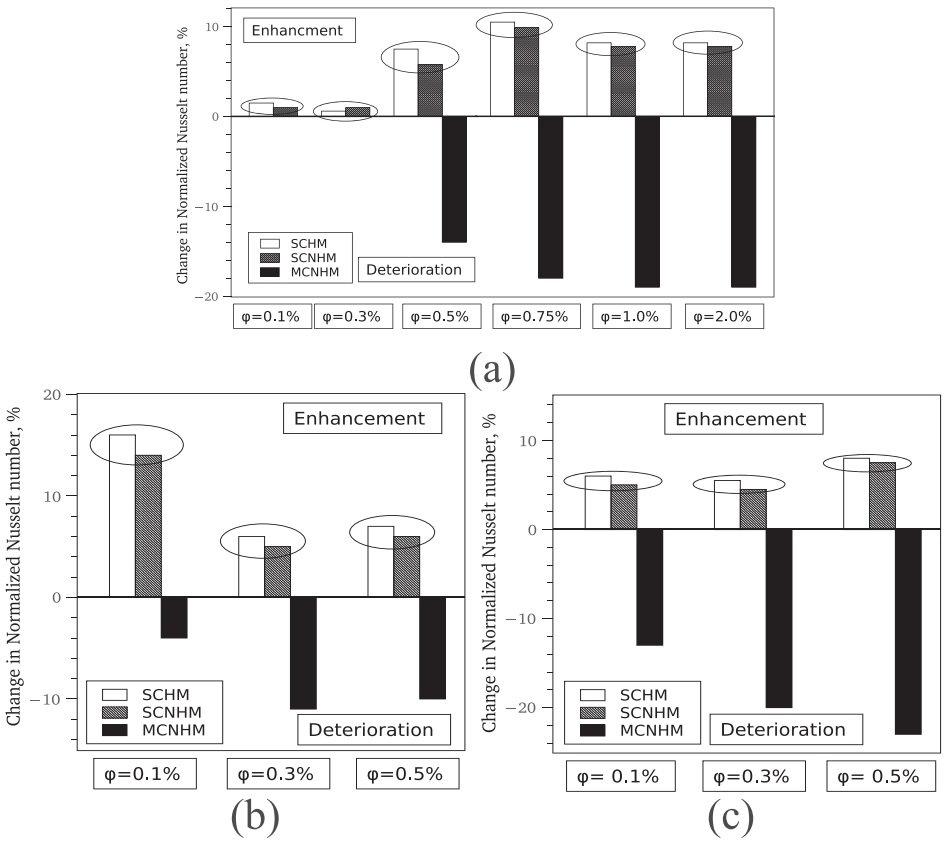


FIG. 9. Percentage deviation in the Nusselt number with different models for (a) alumina/water, (b) MWCNT/water, (c) graphene/water nanofluids at a Rayleigh number of about $1 \times 10^6$.

single model that will predict heat transfer and flow physics for all sets of Rayleigh numbers and volume fractions considered in the present study. Therefore, enhancement seen at lower volume fractions of non-spherical particle-based nanosuspensions cannot be explained quantitatively by any of the three describe models.

Carbon nanotubes having a larger aspect ratio form the percolation chain network as explained in the literature.[14,36] This percolation network when influenced by the temperature gradient perturbs the boundary layer near the wall and thereby increases the local Nusselt number values and causes enhancement. By increasing the volume fraction due to higher particle loading, the effective inertia of the MWCNT chain increases which in turn results in lesser rotation of the MWCNT chains along with the flow of basefluid. Also, with increase in volume fraction, drag becomes a prominent force and thereby causes further deterioration.

Schematics of the chain network formed in MWCNT/water and graphene/water nanofluids along with representation of a dispersed spherical type alumina particle in basefluid are shown in Fig. 10.

Similarly, graphene flakes also form the chain network which causes the heat transfer at lower volume fractions. Graphene flakes are divided into two types: one which are very small and another one which are having a larger area and aspect ratio. Flakes with small sizes behave similar to

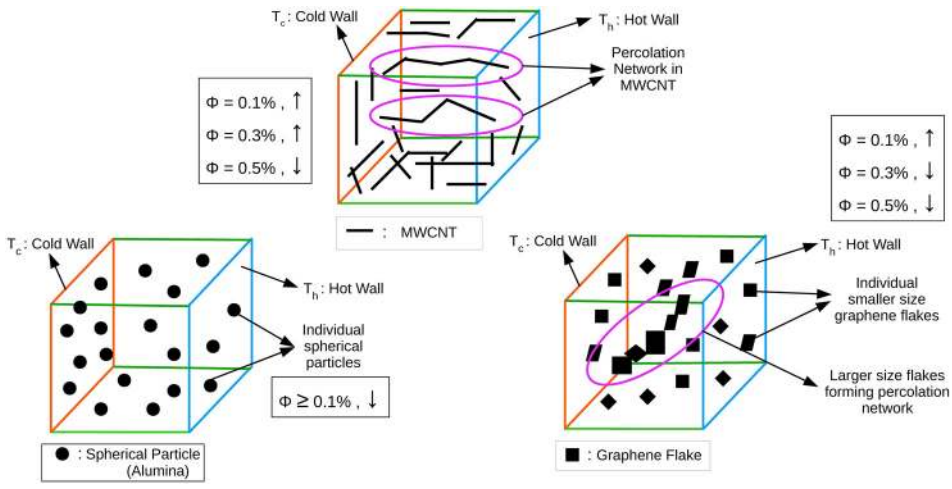


FIG. 10. Schematics of different nanosuspensions. The percolation network of MWCNT in MWCNT/water nanofluid. Larger size flakes of graphene also form percolation networks. The arrows are used with the volume fraction $\phi$ to denote the enhancement (up arrow) or deterioration (down arrow).

those of spherical particles, and those having a larger aspect ratio form a percolation chain similar to MWCNT. Percolation networks in graphene are lesser in number and weaker than the of MWCNT (carbon nanotube) and thus the effect of boundary layer breaking and thereby causing enhancement is only seen at the lowest volume fraction. As volume fraction increases, the percolation network is not sufficient to overcome the effect of a decrease in buoyancy and causes deterioration immediately.

From the present experiments and numerical analysis, it has been observed that MWCNT/water nanofluid performs better than the basefluid, alumina/water, and graphene/water nanofluids at $Ra = 10^6$ for all volume fractions. On the other hand, graphene/water nanofluid shows superior performance than basefluid and alumina/water nanofluid but is not found to be better than the MWCNT/water nanofluid. It can be inferred that nanofluids do not necessarily lead to a deterioration in heat transfer of natural convection in a cavity as has been previously reported.[7] In the present study, the shapes of nanoparticles are found to play a critical role in altering heat transfer characteristics. For the first time, it has been observed that non-spherical nanoparticles could lead to an enhancement in natural convection heat transfer when dispersed at volume fractions less than 0.3%. At a volume fraction of 0.5% and higher, there is a deterioration in heat transfer implying a strong effect of particle shape. It can also be inferred from the present study that the validity of the single component models which do not account for the slip forces is confined to a smaller range of nanoparticle volume fractions as far the non-spherical nanoparticles are concerned. However, for the spherical nanoparticles, these models are showing satisfactory prediction for an extended range of nanoparticle volume fractions up to 0.75%. Thus the role of slip forces is predominant in the case of tubular- and flake-based nanoparticle suspensions.

## VI. SUMMARY AND CONCLUSIONS

From the experiments, we have observed that MWCNT/water is found to be superior in terms of heat transfer enhancement compared to alumina and graphene nanosuspensions. Depending on the volume fraction and shape of the nanoparticles, the heat transfer performance of the nanofluids changes. The major conclusions drawn from the present experimental and numerical investigation for various types of nanosuspensions are as follows:

### A. Alumina/water nanosuspension

Deterioration in heat transfer is experimentally observed for all volume fractions and this deterioration increases with increase in volume fraction. SCHM and SCNHM predict the Nusselt number values very well for lower volume fractions up to 0.5%. For higher volume fractions of 0.75% and above, both SCHM and SCNHM fail to predict the deterioration and so the study of slip mechanisms becomes necessary. MCNHM, which considers all slip mechanisms, predicts deterioration very well for the volume fraction of 0.75% and above. This is because of the inclusion of the drag force into it which is a prominent slip mechanism at higher volume fractions.

### B. MWCNT/water nanosuspension

Enhancement in heat transfer is observed experimentally at the volume fractions of 0.1% and 0.3%, while deterioration is observed at 0.5% of volume fraction. SCHM and SCNHM are closer to experimental observations qualitatively at volume fractions of 0.1% and 0.3%, while for higher volume fractions, both the SCHM and SCNHM overpredict the experimental results. MCNHM shows deterioration for all ranges of volume fractions and becomes closer to the experimental observation at volume fractions of 0.5%; this is due to an increase in the drag force at higher volume fractions which is modeled only in MCNHM. It is seen that enhancement captured numerically at lower volume fractions is a mere coincidence with experimental observations, as it is an inherent characteristic of SCHM and SCNHM to always depict enhancement irrespective of the type of nanofluids considered. The possible mechanism for the enhancement of heat transfer at the lower volume fraction is attributed to the percolation network chain formation that perturbs the boundary layer and increases the local Nusselt number values. For higher volume fractions, the buoyant force becomes less dominant and the effect of boundary layer breaking diminishes thereby resulting in deterioration.

### C. Graphene/water nanosuspension

Experimentally enhancement in heat transfer is observed in the volume fraction of 0.1%, while there is deterioration at higher volume fractions of 0.3% and 0.5%. Similar to the MWCNT/water nanofluid, the enhancement captured by SCHM and SCNHM at the lowest volume fraction of 0.1% is a mere coincidence as SCHM and SCNHM report enhancement at all volume fractions as already explained. For higher volume fractions of 0.3% and 0.5%, MCNHM is in good agreement with the present experimental results due to the inclusion of the drag-based slip force into it. Like MWCNT, graphene flakes with a higher aspect ratio also forms percolation networks which cause enhancement due to boundary layer breaking, but the strength of network chains is lesser compared to MWCNT. And thus, enhancement is only seen at lowest volume fractions. As soon as the volume fraction increased to 0.3%, buoyancy force reduces and thereby causes deterioration. For 0.5% of volume fractions, heat transfer deteriorates still further.

Thus it can be inferred that SCHM and SCNHM are better at volume fractions less than 0.3%, while MCNHM is closer to experimental observations at higher volume fractions. There is no single model which predicts Nusselt number values for all ranges of volume fraction and the types of nanofluids considered alone. And thus molecular dynamic like simulation is required for predicting the actual flow physics and heat transfer characteristics in nanosuspensions.

## ACKNOWLEDGMENTS

The authors gratefully acknowledge Computer Center facility at Indian Institute of Technology Madras for providing Virgo supercomputer required for the present simulation.

[1] S. Li and J. Eastman, "Measuring thermal conductivity of fluids containing oxide nanoparticles," J. Heat Transfer. **121**(2), 280–289 (1999).

[2] S. Choi, Z. Zhang, W. Yu, F. Lockwood, and E. Grulke, "Anomalous thermal conductivity enhancement in nanotube suspensions," Appl. Phys. Lett. **79**(14), 2252–2254 (2001).

[3] H. E. Patel, T. Sundararajan, and S. K. Das, "An experimental investigation into the thermal conductivity enhancement in oxide and metallic nanofluids," J. Nanopart. Res. **12**(3), 1015–1031 (2010).

[4] S. S. Gupta, V. M. Siva, S. Krishnan, T. Sreeprasad, P. K. Singh, T. Pradeep, and S. K. Das, "Thermal conductivity enhancement of nanofluids containing graphene nanosheets," J. Appl. Phys. **110**(8), 084302 (2011).

[5] W.-Q. L. Chengzhen Sun, B. Bai, and J. Liu, "Shear-rate dependent effective thermal conductivity of $H_2O$+$SiO_2$ nanofluids," Phys. Fluids **25**(5), 052002 (2013).

[6] N. Putra, P. Thiesen, W. Roetzel *et al.*, "Temperature dependence of thermal conductivity enhancement for nanofluids," J. Heat Transfer **125**, 567–574 (2003).

[7] C. Ho, W. Liu, Y. Chang, and C. Lin, "Natural convection heat transfer of alumina-water nanofluid in vertical square enclosures: An experimental study," Int. J. Therm. Sci. **49**(8), 1345–1353 (2010).

[8] C. H. Li and G. Peterson, "Experimental studies of natural convection heat transfer of $Al_2O_3$/DI water nanoparticle suspensions (nanofluids)," Adv. Mech. Eng. **2**, 742739 (2010).

[9] Y. Hu, Y. He, S. Wang, Q. Wang, and H. I. Schlaberg, "Experimental and numerical investigation on natural convection heat transfer of $TiO_2$–water nanofluids in a square enclosure," J. Heat Transfer **136**(2) 022502 (2014).

[10] D. Wen and Y. Ding, "Formulation of nanofluids for natural convective heat transfer applications," Int. J. Heat Fluid Flow **26**(6), 855–864 (2005).

[11] S.-Q. Z. Rui Ni and K.-Q. Xia, "An experimental investigation of turbulent thermal convection in water-based alumina nanofluid," Phys. Fluids **23**(2), 022005 (2011).

[12] L. Yang, H. Zhang, G. Zhang, Y. Li, P. Zhang, X. Li, and F. Song, "Experimental study of natural convection heat transfer of $TiO_2$/ethylene glycol nanofluids," Nanosci. Nanotechnol. Lett. **7**(4), 338–346 (2015).

[13] P. S. Joshi and A. Pattamatta, "Buoyancy induced convective heat transfer in particle, tubular and flake type of nanoparticle suspensions," Int. J. Therm. Sci. **122**(Supplement C), 1–11 (2017).

[14] A. Mohamad, "Myth about nano-fluid heat transfer enhancement," Int. J. Heat Mass Transfer **86**, 397–403 (2015).

[15] K. Khanafer, K. Vafai, and M. Lightstone, "Buoyancy-driven heat transfer enhancement in a two-dimensional enclosure utilizing nanofluids," Int. J. Heat Mass Transfer **46**(19), 3639–3653 (2003).

[16] J. Kim, Y. T. Kang, and C. K. Choi, "Analysis of convective instability and heat transfer characteristics of nanofluids," Phys. Fluids **16**(7) 2395–2401 (2004).

[17] C.-J. Ho, M. Chen, and Z. Li, "Numerical simulation of natural convection of nanofluid in a square enclosure: Effects due to uncertainties of viscosity and thermal conductivity," Int. J. Heat Mass Transfer **51**(17), 4506–4516 (2008).

[18] A. K. Santra, S. Sen, and N. Chakraborty, "Study of heat transfer augmentation in a differentially heated square cavity using copper–water nanofluid," Int. J. Therm. Sci. **47**(9), 1113–1122 (2008).

[19] K. S. Hwang, J.-H. Lee, and S. P. Jang, "Buoyancy-driven heat transfer of water-based $Al_2O_3$ nanofluids in a rectangular cavity," Int. J. Heat Mass Transfer **50**(19), 4003–4010 (2007).

[20] D. Tzou, "Thermal instability of nanofluids in natural convection," Int. J. Heat Mass Transfer **51**(11), 2967–2979 (2008).

[21] M. Celli, "Non-homogeneous model for a side heated square cavity filled with a nanofluid," Int. J. Heat Fluid Flow **44**, 327–335 (2013).

[22] A. Avramenko, D. Blinov, and I. Shevchuk, "Self-similar analysis of fluid flow and heat-mass transfer of nanofluids in boundary layer," Phys. Fluids **23**(8), 082002 (2011).

[23] S.-K. Choi, S.-O. Kim, T.-H. Lee, and Dohee-Hahn, "Computation of the natural convection of nanofluid in a square cavity with homogeneous and nonhomogeneous models," Numer. Heat Transfer, Part A **65**(4), 287–301 (2014).

[24] S. Savithiri, A. Pattamatta, and S. K. Das, "A single-component nonhomogeneous lattice Boltzmann model for natural convection in $Al_2O_3$/water nanofluid," Numer. Heat Transfer, Part A **68**(10), 1106–1124 (2015).

[25] C. Qi, Y. He, S. Yan, F. Tian, and Y. Hu, "Numerical simulation of natural convection in a square enclosure filled with nanofluid using the two-phase lattice Boltzmann method," Nanoscale Res. Lett. **8**(1), 56 (2013).

[26] S. Savithiri, P. Dhar, A. Pattamatta, and S. K. Das, "Particle–fluid interactivity reduces buoyancy-driven thermal transport in nanosuspensions: A multi-component lattice Boltzmann approach," Numer. Heat Transfer, Part A **70**(3), 260–281 (2016).

[27] Y. Xuan and W. Roetzel, "Conceptions for heat transfer correlation of nanofluids," Int. J. Heat Mass transfer **43**(19), 3701–3707 (2000).

[28] A. Nnanna, "Experimental model of temperature-driven nanofluid," J. Heat Transfer **129**(6), 697–704 (2007).

[29] D. Yoon, Y.-W. Son, and H. Cheong, "Negative thermal expansion coefficient of graphene measured by Raman spectroscopy," Nano Lett. **11**(8), 3227–3231 (2011).

[30] Zahari, "Thermal properties and heat transfer study of dispersed fluid with functionalized multiwalled carbon nanotube particles," Ph.D. thesis, Universiti Teknikal Malaysia Melaka, 2015.

[31] L. Deng, R. J. Young, I. A. Kinloch, R. Sun, G. Zhang, L. Noé, and M. Monthioux, "Coefficient of thermal expansion of carbon nanotubes measured by Raman spectroscopy," Appl. Phys. Lett. **104**(5), 051907 (2014).

[32] C. J. Greenshields, OpenFOAM User Guide, 2015.

[33] J. Buongiorno, "Convective transport in nanofluids," J. Heat Transfer **128**(3), 240–250 (2006).

[34] A. FLUENT, Theory Guide Release 16.1, 2015.

[35] V. Bianco, F. Chiacchio, O. Manca, and S. Nardini, "Numerical investigation of nanofluids forced convection in circular tubes," Appl. Therm. Eng. **29**(17), 3632–3642 (2009).

[36] P. Dhar, S. Sen Gupta, S. Chakraborty, A. Pattamatta, and S. K. Das, "The role of percolation and sheet dynamics during heat conduction in polydispersed graphene nanofluids," Appl. Phys. Lett. **102**(16), 163114 (2013).